

NUMERICAL SIMULATIONS OF COMPRESSIBLE TURBULENT FLOWS OVER AIRFOILS

Oscar Mauricio Arias Garcia, oscar@ita.br

Nide G. C. R. Fico Jr, nide@ita.br

Technological Institute of Aeronautics. Aeronautical Department.

Abstract. A computer code was developed from scratch to simulate the flow over the NACA 0012 airfoil at different Reynolds and Mach numbers. The domain was discretized in a structured-grid context. The equations were numerically solved by a finite-volume technique, and the use of a Runge-Kutta time-marching technique that respects the direction of the flow. First, the Euler flow was initially modeled as well as a Reynolds-averaged Navier Stokes formulation was calculated. The inviscid NACA 0012 simulation was compared with other numerical results available in the literature. Finally, two compressible, turbulent viscous flows over the NACA 0012 airfoil were numerically solved using the Baldwin & Lomax turbulence model. The pressure coefficient distribution along the airfoil chord and the normal force coefficient were compared with experimental data.

Key words: NACA 0012, Finite volumes, Euler, Navier-Stokes, Turbulence.

Nomenclature

M_∞	Freestream Mach number
p_∞	Static pressure
Δt	Time step for each cell
\bar{U}	Velocity vector
Q	Vector of conserved variables
E, F	Flux vectors in the x and y directions respectively
$T_{i,j}$	Total flux across the control volume
$P_{i,j}$	Super vector containing the inviscid and viscous fluxes
$V_{i,j}$	Cell volume

1. INTRODUCTION.

The present report deals with both Euler and Navier-Stokes simulations. Its first phase, constituted of inviscid simulation, was performed over a NACA 0012 airfoil at an angle of attack of 1.25, a very challenging simulation because of the presence of shock waves. The pressure coefficient result was compared with those from other authors. The next step was to introduce the viscous terms and thus provide physical diffusivity to the flow model. Full viscous turbulent simulations over the NACA 0012 airfoil were performed. The nature of the flow is almost fully turbulent due to the flow high Reynolds numbers. Thus, the Baldwin and Lomax (1978) turbulence model was used. Two cases were simulated. In the first one the free stream Mach number, M_∞ , was equal to 0.5 and the Reynolds number based upon the airfoil chord, Re_c , was set to 3×10^6 . Next, the Reynolds number was increased to 9×10^6 and the incoming flow Mach number was set to $M_\infty = 0.74$. The structured grid was carefully generated to properly capture the turbulent boundary layer. For every viscous case, the pressure coefficient distribution and normal force coefficient were compared to the experimental values of Harris (1981).

2. NUMERICAL FORMULATION.

The rate of change of a general flow variable ϕ within a finite control volume can be expressed as a balance among the net convective and diffusive fluxes and the net creation of ϕ within the control volume (Versteeg and Malalasekera, 1995). Therefore,

$$\left[\begin{array}{l} \text{Rate of change of} \\ \phi \text{ in the control} \\ \text{volume with} \\ \text{respect to time} \end{array} \right] = \left[\begin{array}{l} \text{Net flux of } \phi \\ \text{due to convection} \\ \text{into the control} \\ \text{volume} \end{array} \right] + \left[\begin{array}{l} \text{Net flux of } \phi \\ \text{due to diffusion} \\ \text{into the control} \\ \text{volume} \end{array} \right] + \left[\begin{array}{l} \text{Net rate of} \\ \text{creation of } \phi \\ \text{inside the} \\ \text{control volume} \end{array} \right] \quad (1)$$

Integrating the flow equations for each surface of the cell control volume we have

$$\frac{\partial Q_{i,j}}{\partial t} = -\frac{1}{V_{i,j}} \int_{S_{i,j}} (\vec{P} \cdot \vec{n}) dS, \quad (2)$$

where $V_{i,j}$ is the cell volume, $S_{i,j}$ is the surface of the control volume, and \vec{P} is given by

$$\vec{P} = E\vec{i}_x + F\vec{i}_y, \quad (3)$$

where E and F are the flux vectors in the x and y directions, respectively, while \vec{i}_x and \vec{i}_y are Cartesian unit vectors.

The fluxes across the grid-cell surface are calculated by averaging the flow properties on both sides, giving rise to a central-discretization scheme. To advance the solution in time Jameson suggested a five-stage Runge-Kutta integration scheme. The dissipative fluxes are calculated in all the Runge-Kutta stages to improve the stability. Thus, adding the numerical dissipation operator to Eq. (2), one gets:

$$\frac{\partial Q_{i,j}}{\partial t} + \frac{1}{V_{i,j}} [T(Q_{i,j}) - Da(Q_{i,j})] = 0 \quad (4)$$

where $T(Q_{i,j})$ is the discrete approximation of all the fluxes crossing the surface of the control volume and $Da(Q_{i,j})$ denotes the artificial viscosity. Let the superscript n denote the time level. Thus, $n+1$ represents the next time level after a time increment equal to Δt . To advance the calculation towards the steady state solution, one writes:

$$\begin{aligned} Q^{(0)} &= Q^n, \\ Q^{(1)} &= Q^{(0)} - \alpha_1 \frac{\Delta t}{V_{i,j}} [T_e(Q^{(0)}) - Da(Q^{(0)})], \\ Q^{(2)} &= Q^{(0)} - \alpha_2 \frac{\Delta t}{V_{i,j}} [T_e(Q^{(1)}) - Da(Q^{(1)})], \\ Q^{(3)} &= Q^{(0)} - \alpha_3 \frac{\Delta t}{V_{i,j}} [T_e(Q^{(2)}) - Da(Q^{(2)})], \\ Q^{(4)} &= Q^{(0)} - \alpha_4 \frac{\Delta t}{V_{i,j}} [T_e(Q^{(3)}) - Da(Q^{(3)})], \\ Q^{(5)} &= Q^{(0)} - \alpha_5 \frac{\Delta t}{V_{i,j}} [T_e(Q^{(4)}) - Da(Q^{(4)})], \\ Q^{n+1} &= Q^{(5)}. \end{aligned} \quad (5)$$

where the subscripts i,j in the Q vector were neglected for simplicity. The standard values for the α coefficients, used in the present work, are $\alpha_1 = \frac{1}{4}$, $\alpha_2 = \frac{1}{6}$, $\alpha_3 = \frac{3}{8}$, $\alpha_4 = \frac{1}{2}$ and $\alpha_5 = 1$.

2.1 Non-linear artificial viscosity

The artificial dissipative terms used here is a non-linear formulation proposed by Jameson *et al* (1981). The construction of the non-dissipative linear terms for each variable, in this case for the density is:

$$D\rho = D_x\rho + D_y\rho. \quad (6)$$

where: $D_x\rho$ and $D_y\rho$ are corresponding contributions for the two coordinates directions. Written in conservation form:

$$D_x\rho = d_{i+1/2,j} - d_{i-1/2,j} \quad \text{and} \quad D_y\rho = d_{i,j+1/2} - d_{i,j-1/2}. \quad (7)$$

In Eq. (7), the terms on the right all have a similar form:

$$d_{i+1/2,j} = \frac{V_{i+1/2,j}}{\Delta t} \left\{ \varepsilon_{i+1/2,j}^{(2)} (\rho_{i+1,j} - \rho_{i,j}) - \varepsilon_{i+1/2,j}^{(4)} (\rho_{i+2,j} - 3\rho_{i+1,j} + 3\rho_{i,j} - \rho_{i-1,j}) \right\}. \quad (8)$$

where $V_{i,j}$ is the cell volume, and the coefficients $\varepsilon^{(2)}$ and $\varepsilon^{(4)}$ are dependent on the user-defined constants $k^{(2)}$ and $k^{(4)}$, and on a pressure sensor defined as:

$$\delta p_{i,j} = \frac{|p_{i+1,j} - 2p_{i,j} + p_{i-1,j}|}{|p_{i+1,j}| + 2|p_{i,j}| + |p_{i-1,j}|}. \quad (9)$$

Then

$$\varepsilon_{i+1/2,j}^{(2)} = k^{(2)} \max(\delta p_{i+1,j}, \delta p_{i,j}) \quad \text{and} \quad \varepsilon_{i+1/2,j}^{(4)} = \max\left(0, \left(k^{(4)} - \varepsilon_{i+1/2,j}^{(2)}\right)\right). \quad (10)$$

The standard values of the constants $k^{(2)}$ and $k^{(4)}$ are

$$k^{(2)} = \frac{1}{4}, \quad k^{(4)} = \frac{1}{256}.$$

The dissipative terms for the remaining equations are obtained by substituting ρu , ρv and e for ρ in these formulas.

2.2 Grid details

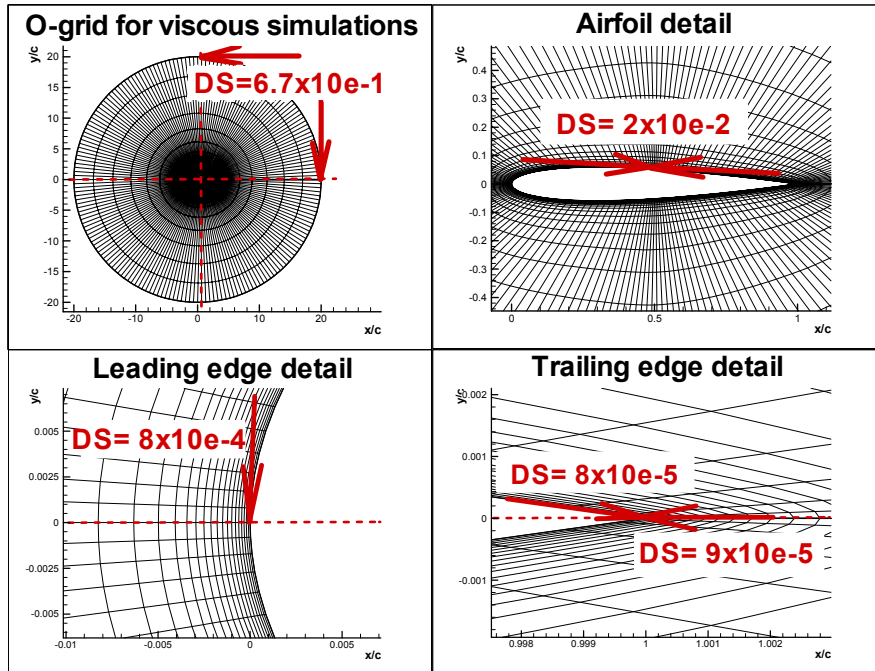


Figure 1: Grid details for viscous simulations.

The computational mesh appearing in Fig. 1 was very carefully constructed. This grid was used for the Navier-Stokes simulations. The minimum non-dimensional distance from the wall to the closest point at the leading and trailing edges, DS , is highlighted. The mesh had 189 by 43 grid points along i -direction- and j -direction respectively. For the Euler cases a similar grid, but with less point close to the airfoil surface, was used.

3. RESULTS

3.1. Inviscid simulation over the NACA 0012

The pressure coefficient, shown in Fig. 2 looks similar as that provided by Pulliam (1986), using a finite difference method. The minimum pressure coefficient value at the upper surface was found to be approximated -1.1 for both solutions. The present result is compatible to that of other authors. However, the shock wave was shifted towards the leading edge, as reported by Wenneker (2002) on his doctoral thesis. This happens because of the entropy generation at the leading edge, which creates a ‘numerical boundary layer’, causing losses (close to the airfoil) that are visible in the constant Mach lines, see Fig. 3.

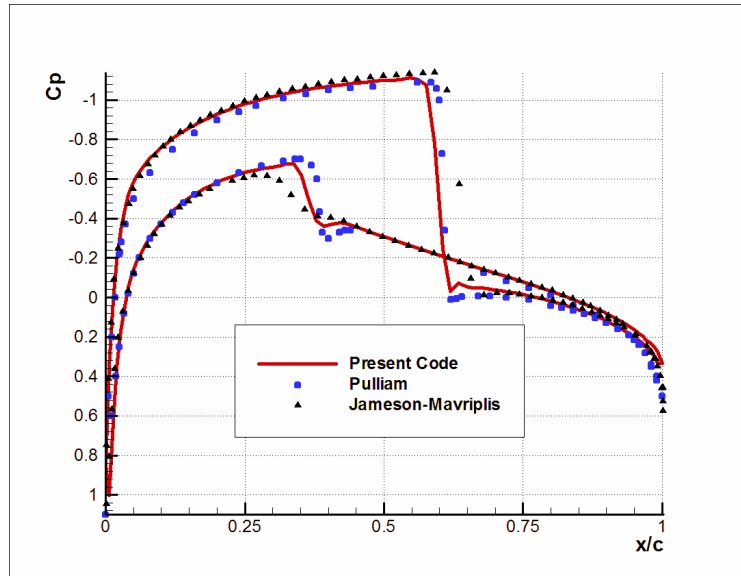


Figure 2: Comparison for the C_p along the airfoil chord for $M_\infty=0.8$, $\alpha=1.25$.

The weak shock wave, at the lower part of the airfoil, is particularly hard to capture. There was a difference in the lower shock, for the code it looks thicker, starting at x/c equal to 0.33, just four percent ahead of the Pulliam result. This difference may be related to two possible reasons: one is the AV coefficients combined with the type of grid used by Pulliam, and the other is the use by Pulliam of upwind differencing in supersonic regions, as suggested by Steger (1978), producing better shock capturing capabilities. In this work a central-discretization scheme was used.

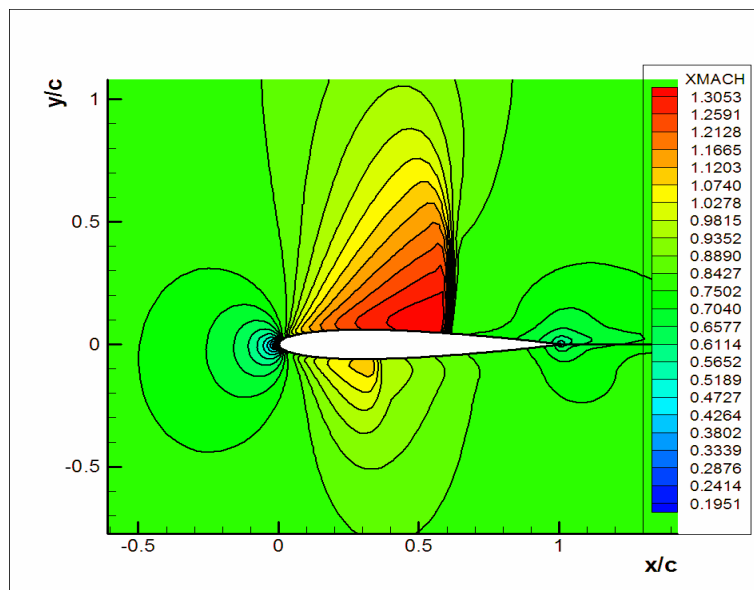


Figure 3: Mach contours for $M_\infty=0.8$, $\alpha=1.25$.

3.2. Turbulent Viscous Flow over the NACA 0012

3.2.1. Mach number: 0.5, angle of attack: 5.86.

The next simulation of the flow over the NACA 0012 airfoil was for a free-stream Mach number, M_∞ , equal to 0.5. The Reynolds number, based on the airfoil chord, was equal to 3×10^6 . For all viscous simulations the starting point was an intermediate Euler solution obtained after 10,000 iterations. Then the viscous terms were switched on. This was done in order to reduce computational processing time. The CFL numbers of the Euler and NS simulations were 0.3 and 0.2 respectively. The artificial viscosity coefficients were set to $K_2 = 1.0$ and $K_4 = 0.05$ for both phases of the computations. The y^+ value at $j=2$ was under 3, along the whole airfoil.

For this particular simulation, the difference between the inviscid and viscous solution was evident. This result is presented without wall interference corrections reported by Harris (1981). The numerical result was in a very good agreement with the experiment along most of the airfoil chord. There was, indeed, a small deviation close to the leading edge; this can be clearly seen in Fig. 4.

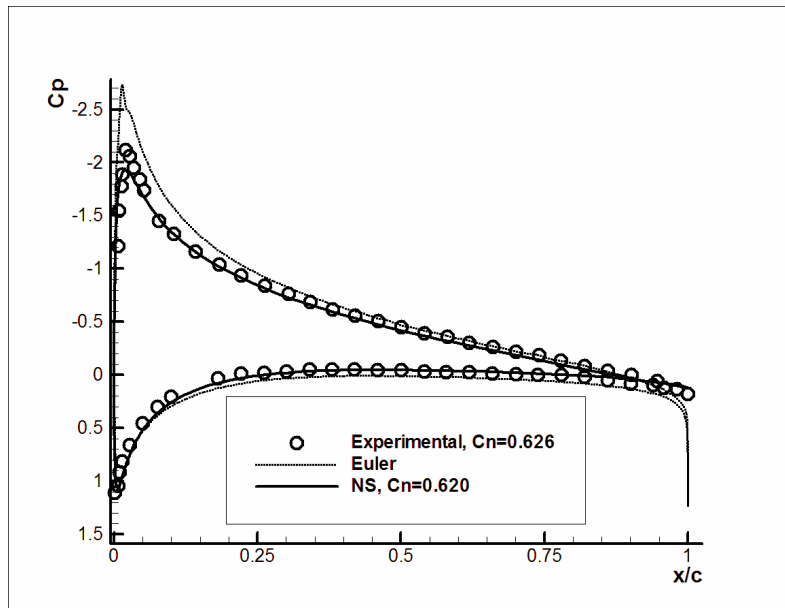


Figure 4: Pressure distribution for $M_\infty=0.5$ and $\alpha=5.86$.

The Euler numerical result showed a steeper suction peak, while for the Navier-Stokes simulations the suction peak was a little underestimated. However, despite this minor departure from the experimental C_p data, the normal force coefficient was found to be $C_n = 0.620$. Comparing with experimental data, $C_n = 0.626$, the error is less than one percent. There may be numerical issues associated with the small differences on the C_p results. Many different grids and artificial viscosity coefficients were tried prior to the combination that yielded the solution presented here. For example, numerical tests were performed with less artificial viscosity. It was found that, On one hand, the pressure coefficient distribution seemed to be even closer to the data due to Harris(1981). But, on the other hand, the normal force coefficient error increased to values as high as 9 %. Pressure and Mach contours, with $K_2 = 1.0$ and $K_4 = 0.035$, are presented in fig. (5) and (6), respectively. The isolines contours were free of distortion.

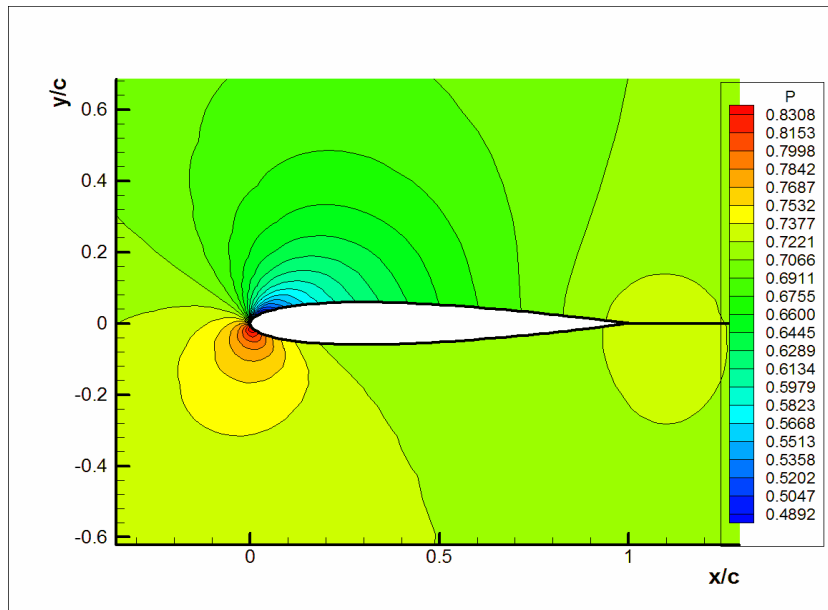


Figure 5: Pressure contours for $M_\infty=0.5$ and $\alpha=5.86$.

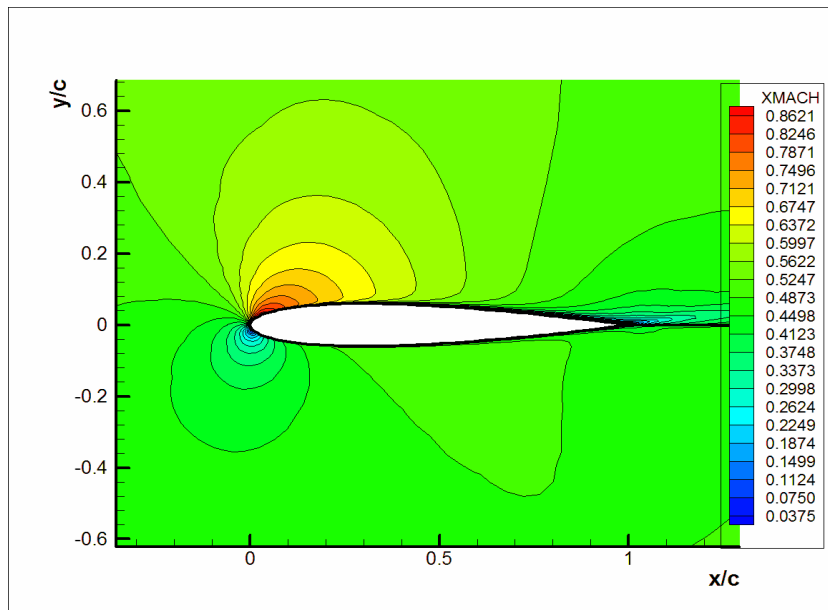


Figure 6: Mach contours for $M_\infty=0.5$ and $\alpha=5.86$.

The residue for the density variation showed a plateau for the inviscid calculation. For Navier-Stokes, despite some discrete peaks, the overall trend was always towards convergence, see Fig. 7. At 40,000 iterations the normal force variation is very small, but the density convergence is only obtained after 48,964 iterations.

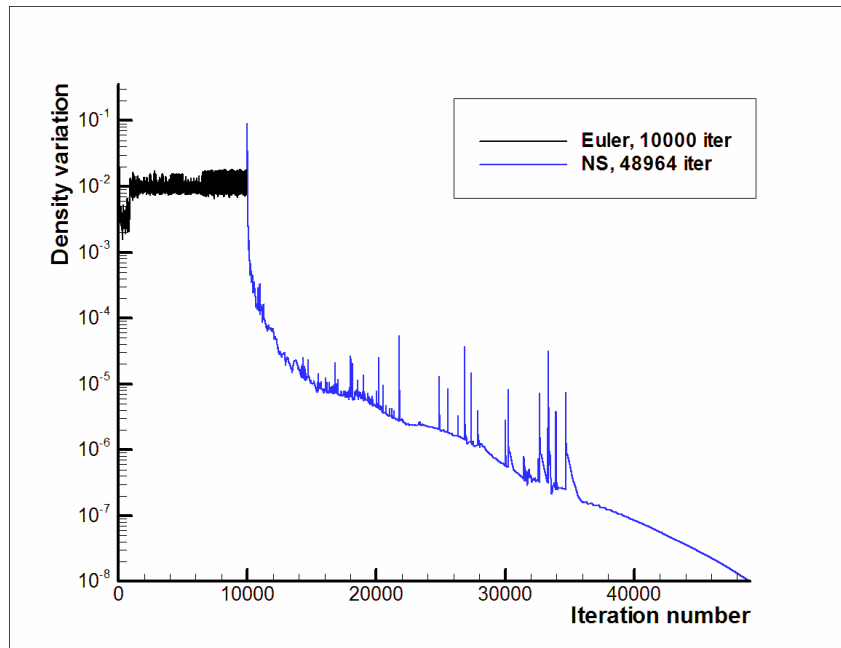


Figure 7: Density variation history for $M_\infty = 0.5$ and $\alpha = 5.86$.

3.2.2. Mach number: 0.74, angle of attack: -0.14.

The next simulation was for a free-stream Mach number, M_∞ , equal to 0.74. The Reynolds number, based on the airfoil chord, was equal to 9×10^6 . The angle of attack, α , was -0.14. The CFL number for the Euler simulation was the same as for the previous case. The CFL number for the Navier-Stokes simulation was lowered to 0.18. The non-linear AV coefficients were $K_2 = 1.0$ and $K_4 = 0.02$.

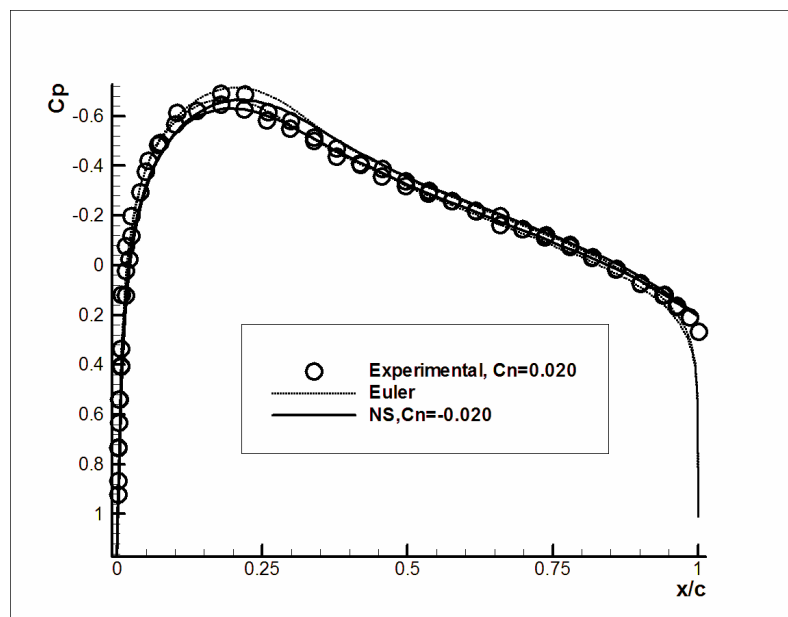


Figure 8: Pressure Coefficient for $M_\infty = 0.74$ and $\alpha = -0.14$.

The experimental C_p value was found to be -0.69, while for the Navier-Stokes numerical simulation result the suction peak was -0.66 as shown in Fig. 8. Although much smaller, there was also a difference, between the numerical and the experimental data, at the airfoil lower surface. The numerical C_p result was slightly greater than the experimental value from the leading edge to about $x/c = 0.1$. This may be related to the fact that the boundary layer is

very thin, at this zone, and therefore grid is too coarse to capture it correctly. In spite of this differences, the value of the normal force coefficient was exactly the same reported by the experimental information, that is, $C_n = 0.020$.

Pressure and Mach contours are present in Fig. 9 and 10. The maximum Mach number at the upper surface of the airfoil was 0.99, located at $x/c = 0.194$. The lower surface achieve the sonic speed at $x/c = 0.196$. However, no shock wave was formed.

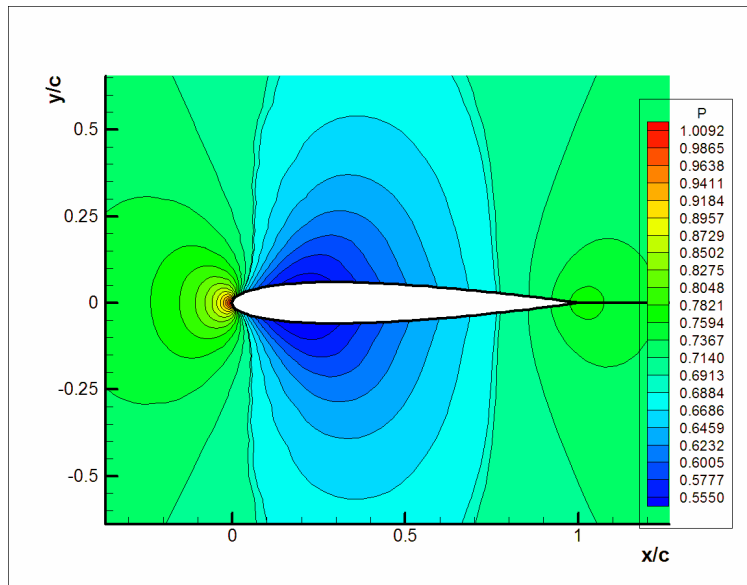


Figure 9: Pressure Contours for $M_\infty = 0.74$ and $\alpha = -0.14$.

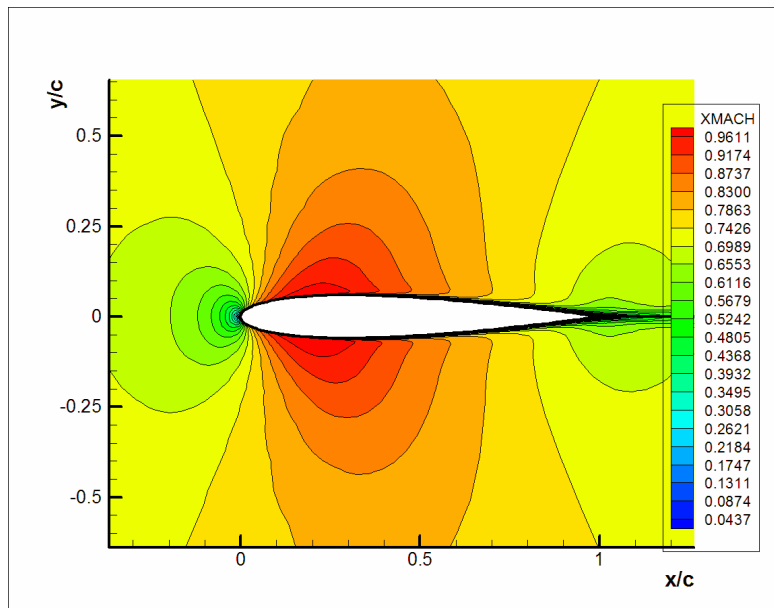


Figure 10: Mach contours for $M_\infty = 0.74$ and $\alpha = -0.14$.

The density convergence rate is shown for both, partial Euler and Navier-Stokes simulations in Fig. 11. The convergence criterion was attained with 58,547 iterations, but after 30,000 there was no a significance change on the flow properties.

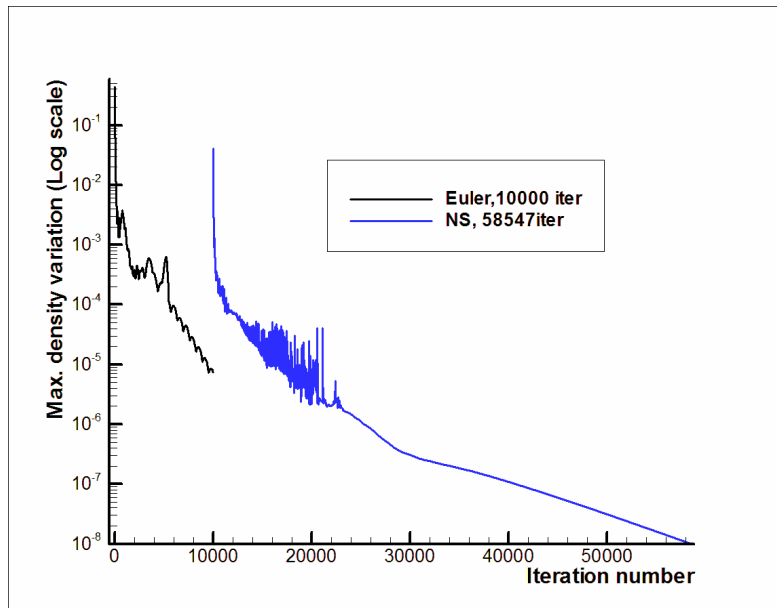


Figure 11: Density variation history for $M_\infty=0.7$ and $\alpha=1.86$.

4. CONCLUSIONS

The code implemented in the present work, proved to be very robust for both Euler and turbulent Navier-Stokes simulations. It is important to do an even more careful study of the influence of the artificial viscosity influence on the final result of the simulation. It was observed that the AV coefficients modified not only the convergence rate, but also the converged result. Thus, it is imperative to study deeper the numerical-viscosity schemes and its influence on the result.

Moreover, Jameson's scheme allows for greater CFL numbers, which could, at least in part, compensate the larger number of iterations it needs to converge, as well as, the more computer intense calculations between time steps comparing with other techniques. For the Navier-Stokes simulations, the use of a Runge-Kutta time-marching technique that respects the direction of the flow could increase the maximum allowable CFL number. For example, in the NACA 0012 simulations, the Runge-Kutta cycles were divided in two, one for the upper surface and another for the lower surface of the airfoil, respecting the preferable direction of the convective terms.

5. REFERENCES

- Baldwin, B. S.; Lomax, H. "Thin layer approximation and algebraic model for separated turbulent flows". In: Aerospace Sciences Meeting, 16., 1978, Huntsville. Proceedings... Huntsville: AIAA, 1978. p.78-257.
- Harris, Charles, D. "Two-dimensional aerodynamic characteristics of the NACA 0012 airfoil in the langley 8 foot transonic pressure tunnel". Langley Research Center: NASA, 1981. (NASA Technical Memorandum, 81927).
- Jameson, A.; Schmidt, W.; Turkel, E. "Numerical solution of the Euler Equations by finite volume methods using runge-kutta time-stepping schemes". In: FLUID AND PLASMA DYNAMICS CONFERENCE, 14., 1981, Palo Alto. Palo Alto: AIAA, 1981. Paper No.81-1259
- Pulliam, Thomas. "Artificial dissipation models for Euler equations". AIAA Journal, v. 24, n. 12, p. 1931-1940, december, 1986.
- Steger, J. L. "Implicit finite difference simulation of flow about arbitrary geometries with applications to airfoils". AIAA Journal, v. 16, p. 679, Jul., 1978.
- Versteeg, H.; Malalasekera, W. "An introduction to computational fluid dynamics, the finite volume method". [S.l.]: Longman Group, 1995.
- Wenneker, Ivo. "Computation of flows using unstructured staggered grids". 2002. Thesis. (Doctoral Dissertation) - DELFT University of Technology, Delft, The Netherlands.

6. RESPONSIBILITY NOTICE

The authors are the only responsible for the printed material included in this paper.